MALAYSIAN JOURNAL OF SCIENCE
MJS
ISSN 1394 - 3065

5th International Conference on Applied & Industrial Mathematics and Statistics 2025 (ICoAIMS 2025)

Special Issue

Malaysian Journal of Science 45 (Special Issue 2): 37-42 (November 2026) https://mjs.um.edu.my

Deconvolving Neuronal Ensembles from Macroscopic Neural Activities in Voltage-Sensitive Dye Image Streams on Mouse Cerebrum Slices

Karin Horiuchi[1a], Santa Fukuda[2b], Masahiro Ohtani[3a] and Yuki Hayashida[4b]*

Abstract: Previous clinical trials have demonstrated that electrical microstimulation delivered within the primary visual cortex (V1) in human subjects with acquired blindness can evoke focal light sensations in their visual fields, supporting the feasibility of intracortical visual prostheses. Our previous animal studies using voltage-sensitive dye (VSD) imaging examined the spatiotemporal patterns of cortical neural activity in response to electrical current-pulse stimuli, varying stimulus parameters to optimize stimulation design. These studies revealed specific relationships between stimulus parameters and neural responses at millisecond temporal resolution and submillimeter spatial scales. However, as VSD images typically represent voltage changes across all cytoplasmic membranes of cells responding to stimuli, activities of individual neuron populations and their functional connections are obscured by the macroscopic responses. This study aims to investigate stimulus-induced neuronal activities at a finer spatial resolution by employing image processing techniques. Specifically, spatial and temporal cross-correlation analyses were applied to VSD image streams to identify spatially distinguishable patterns of pixel clusters exhibiting temporally correlated VSD signals. In certain cases, these neuronal ensembles, each smaller than 100 micrometers in diameter, displayed time-fixed correlation in membrane voltage change, suggesting functional connectivity between them. The image processing method demonstrates the potential of separating distinct activities of cortical neuronal ensembles from macroscopic VSD imaging data, offering a valuable tool for detailed studies of stimulus-induced network dynamics and, in turn, optimizing stimuli for visual prostheses.

Keywords: Visual prosthesis, Neuronal ensemble, Voltage-sensitive dye imaging, Spatio-temporal cross-correlation analyses

1. Introduction

Previous clinical trials have demonstrated that electrical stimulation of the primary visual cortex (V1) using tissue-penetrating microelectrodes evokes light perception, termed phosphenes, in the visual field of blind patients (Schmidt et al., 1996; Fernández et al., 2021). This phenomenon highlights the potential of cortical visual prostheses, which allow blind individuals to perceive spots of light. Building on these findings, recent years have witnessed progress in both fundamental research and prosthetic devices (Chen et al., 2020; Hayashida et al., 2022). Since the functionality of intracortical prostheses depends on precisely designed and controlled stimulation, a comprehensive understanding of the physiological basis of neuronal activity responding to these stimuli is essential.

Physiological experiments in rodents, both in vivo and with brain slice preparations, have offered valuable insights into the spatiotemporal characteristics of neural responses to microstimulation in V1. Using the voltage-sensitive dye (VSD) imaging technique, it has been demonstrated that microstimulation pulses can elicit action potentials in neural populations within milliseconds in both sighted and blind animals (Fehérvári et al., 2015; Miyamoto et al., 2017). These population action potentials subsequently trigger focal activation of cortical neural circuits, involving competitive dynamic interactions between excitatory and inhibitory signaling (Tanaka et al., 2019). Moreover, these studies have revealed specific relationships between stimulus parameters and the resulting neural responses (Miyamoto et al., 2017; Tanaka et al., 2019; Hayashida et al., 2022), and they contribute to explaining, for example, the suppressive effects observed in clinical trials when high-frequency pulse-train stimulation was applied (Hayashida et al., 2014; Nomoto et al., 2017; Fukuda et al., 2022).

While VSD imaging in the slice preparation has provided critical insights into neural response dynamics with millisecond temporal resolution and submillimeter spatial scales (Tanaka et al., 2019), it reflects voltage changes across all cytoplasmic membranes of cells responding to stimuli. Consequently, it obscures the activities of individual neuron populations or neuronal elements, leaving many details to be clarified at finer spatial resolutions. In this study, we aim to investigate neuronal responses at microscopic resolution, on the scale of tens of micrometers, by applying image analysis techniques. This approach aims to enhance our understanding of the functional connectivity between neuronal elements in response to microstimulation in V1.

Authors information:
[a]Dept. of Electrical Engineering, National Institute of Technology Nara College, Nara, Japan, E-mail: ae1175@nara.kosen-ac.jp[1]
E-mail: ohtani@elec.nara-k.ac.jp[3]
[b]Dept. Information Engineering, Grad. Engineering, Mie University, Mie, Japan,
E-mail: 423d054@m.mie-u.ac.jp[2]

*Corresponding Author: hayashida@info.mie-u.ac.jp[4]

Received: October 28, 2025
Accepted: May 6, 2026
Published: November 15, 2026

DOI: https://doi.org/10.22452/mjs.vol45sp2.4
Malaysian Journal of Science 45 (Special Issue 2): 37-42 (November 2026)

2. Methods

2.1 Physiological Experiment with VSD Imaging

The Animal Experiment Committee of Mie University approved animal care and experimental procedures in this study. The method of VSD imaging was similar to that used in our previous studies (Tanaka et al., 2019; Fukuda et al., 2021). In brief, cerebral tissue slices (~0.3-mm thick, containing V1) were prepared from a 4-week-old C57BL/6J mouse and stained with VSD, NK3630 (Nippon Kankoh-Shikiso Kenkyusho). A glass micropipette electrode (~6-µm tip diameter, ~1-MΩ tip resistance) was inserted in layer II/III of V1, and a return electrode (Ag/AgCl-pellet) was placed in the recording chamber. A train of cathodic-first biphasic current pulses (20 µA/phase, 0.2 msec/phase, repetition rate of 50 or 200 Hz) was delivered to layer II/III via the electrode. The transmitted light images of a rectangular region along the mediolateral axis within layer II/III (154 × 820 µm on the slice) were captured at 1000 frames per second with 12 × 64 binned pixels using an Electron Multiplying Charge-Coupled Device camera (iXon 3 DU-897, Andor Technology).

2.2 VSD Imaging Data and Image Processing

Data analysis and image processing were carried out using MATLAB (ver. R2024a, MathWorks). The pre-processing of VSD imaging data followed procedures similar to those in our previous study (Tanaka et al., 2019). After averaging across multiple trials of the recording, each pixel value in the image was converted to the relative change in the transmission light intensity, denoted as $\Delta T(t_n)/T_0$ at time t_n . A decrease and an increase in $\Delta T(t_n)/T_0$ correspond to the membrane hyperpolarization and depolarization, respectively. To decrease noise, the converted images were subjected to spatial filtering (Gaussian, 3×3-pixel mask).

Figure 1 presents the workflow for the image processing steps described in this study. The initial step involves subtracting the accumulating component of neural response to the pulse-train stimulus (Fukuda et al., 2021). This step is crucial for isolating local neuronal activities that would otherwise be masked by the global response to the stimulus pulse, and for facilitating the deconvolution of underlying networks in the following analyses. The time course of $\Delta T(t_n)/T_0$ for each image pixel is processed using a 6th-order Bessel low-pass temporal filter with a cutoff frequency of 20 Hz. After the group delay introduced by the filtering is compensated to ensure accurate temporal alignment, the filtered time course is subtracted from the original $\Delta T(t_n)/T_0$ time course. This provides a processed time series of $\Delta T(t_n)/T_0$ images that preserves local neuronal responses at a finer spatial scale.

The second step involved manually selecting spatially clustered pixels that are visually distinguishable from the surrounding pixels in the subtracted time-series images generated by the initial step. For each of the pixel clusters, the processed $\Delta T(t_n)/T_0$ time courses within a 3×3-pixel area were averaged to obtain the corresponding local response time course.

In the third step, the time points during which the local response was either spatially distinct or reached local extrema in time were identified for each pixel cluster. The image frames at these time points were then averaged, producing an image map that highlights specific pixel patterns whose activity correlates with that of the given pixel cluster. This resulting image is referred to as the "spatial correlation map."

In the fourth step, the temporal cross-correlation function between the selected pixel cluster and specific pixels in the spatial correlation map is computed using the local response time courses at these two locations (denoted as $x(t)$ and $y(t)$)). The cross-correlation function $R(\Delta t)$ is defined as:

$$R(\Delta t) = \int_{T_{min}}^{T_{max}} x(t) \cdot y(+\Delta t)\ dt \qquad (1)$$

where Δt represents the time lag between the signals in two locations, T_{min} and T_{max} denote the start and end time points, respectively, of the duration over which the cross-correlation is calculated. The cross-correlation function was then filtered using a 6th-order Bessel low-pass filter with a cutoff frequency of 400 Hz, and the group delay introduced by the filtering was compensated. As an alternative to manually selecting a specific pixel cluster in the second step, if the signal-to-noise ratio in the time course of each pixel is sufficiently high, then all pixels can be included in the subsequent analyses. In this case, temporal cross-correlation functions were first computed between a given reference pixel and every other pixel. Subsequently, the peak amplitudes of these functions were mapped onto a two-

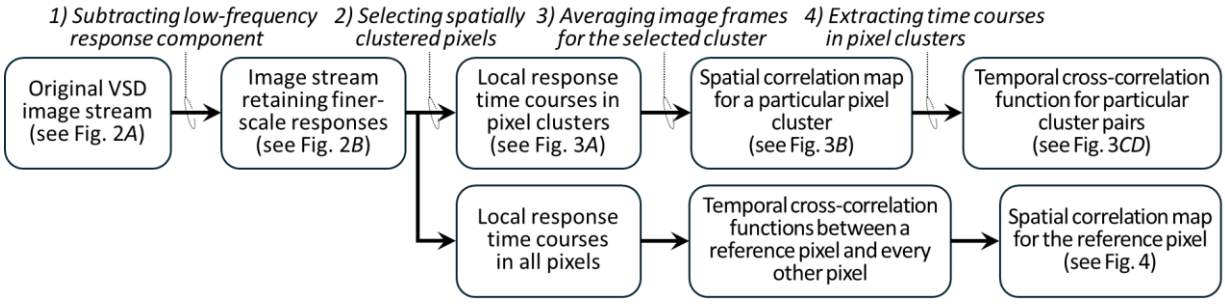


Figure 1. Image processing workflows. The diagram illustrates the four sequential steps.

DOI: https://doi.org/10.22452/mjs.vol45sp2.4
Malaysian Journal of Science 45 (Special Issue 2): 37-42 (November 2026)

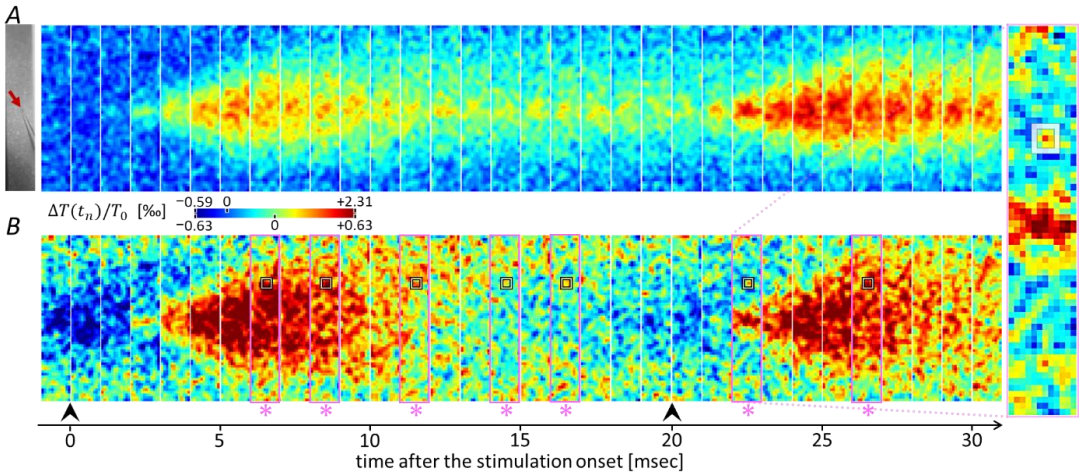


Figure 2. Unmasking local neuronal activities in VSD imaging. *A*) A near-infrared microphotograph of the tissue in the imaging field (left-most) and time-series VSD images (32 image frames) recorded from the tissue in response to stimulus current pulses delivered from the electrode tip inserted in the tissue (indicated by an arrow) at time 0 and 20 msec after the stimulation onset (indicated by arrowheads). *B*) Time-series images generated by subtraction of the low-frequency component from the original images shown in *A*. Asterisks indicate the image frames used for the averaging process. An enlarged view of one of those frames is shown on the right-most. W*hite* squares indicate an example of selected pixel clusters. The color codes differ between *A* and *B*.

dimensional spatial layout corresponding to the pixel locations, resulting in spatial correlation maps for the given pixel (see *lower* workflow in Figure 1).

3. Results

3.1 Local VSD Responses Unmasked from Global Response

Figure 2*A* shows an example of VSD images of the tissue responding to a train of microstimulation pulses (50-Hz repetition rate and 20-μA/phase current amplitude). The leftmost image displays a transmitted image of a portion of the layer II/III of V1, referred to as the imaging field, with the stimulating electrode tip inserted into the tissue at the center of the field (indicated by an arrow). The remaining frames show time-series VSD images in the imaging field using a color-coded scale. Consistent with our previous studies (Tanaka et al., 2019; Fukuda et al., 2021), an increase in $\Delta T(t_n)/T_0$ was observed near the electrode tip within one to two milliseconds after the onset of the stimulus pulse (indicated by an arrowhead at the 0-msec time point), representing action potentials elicited in a neural population (Tanaka et al., 2019). Subsequently, the excitation became more pronounced in amplitude and spatially propagated toward the periphery over the next several milliseconds. This represents synaptic propagations of neural excitation (Tanaka et al., 2019; Fukuda et al., 2021). The response then gradually decayed in both amplitude and spatial extent, reflecting synaptic inhibition of neural activity [6].

In response to the second stimulus pulse (indicated by an arrowhead at the 20-msec time point), $\Delta T(t_n)/T_0$ increased to higher amplitudes than those elicited by the first pulse due to the accumulation of synaptic and non-synaptic responses (Fukuda et al., 2021). These global response characteristics were consistently observed across various tissue slice samples we used in the present and previous studies. On the other hand, the finer-scale spatial patterns of the responses appeared to vary among samples. To visually enhance such local response patterns, a low-frequency response component was subtracted from the original image sequence, resulting in time-series images shown in Figure 2*B*. Compared to the original images (Figure 2*A*), each of these image frames highlights patchy response patterns, with some spatially clustered pixels becoming discernible from the surrounding areas (indicated by white squares as examples). Since their locations were similar across multiple image frames (indicated by asterisks), each pixel cluster was presumed to represent distinct neuronal elements rather than speckle noise.

3.2 Presumed Neuronal Elements Deconvolved in Correlation Map

Figure 3*A-a* shows the "local response time course" (see Figure 1) for the example pixel cluster highlighted in Figure 2*B*. As shown in Figure 3*B-a*, this pixel cluster (indicated by a *green* square) was located about 150 μm from the stimulating electrode tip. Figure 3*B-b* displays the "spatial correlation map" for this pixel cluster (see Figure 1), highlighting a specific pattern of pixels considered to be functionally correlated with the selected pixel cluster. Figure 3*B-c* offers a three-dimensional view of this map, showing another peak with a pixel value comparable to that of the original cluster (indicated by a *grey* arrow, corresponding to the *grey* square in sub-panel *b*). The location of this secondary peak is near the stimulating electrode tip, as shown in subpanel *a* (*grey* square). Figure 3*A-b* represents the local response time course at the location of this secondary peak. The inset depicts a superimposition of the two response time courses at an expanded time scale, confirming repetitive membrane excitations in response to the current pulses at both locations. The stimulus pulses were delivered for a 400-msec duration (indicated by

DOI: https://doi.org/10.22452/mjs.vol45sp2.4
Malaysian Journal of Science 45 (Special Issue 2): 37-42 (November 2026)

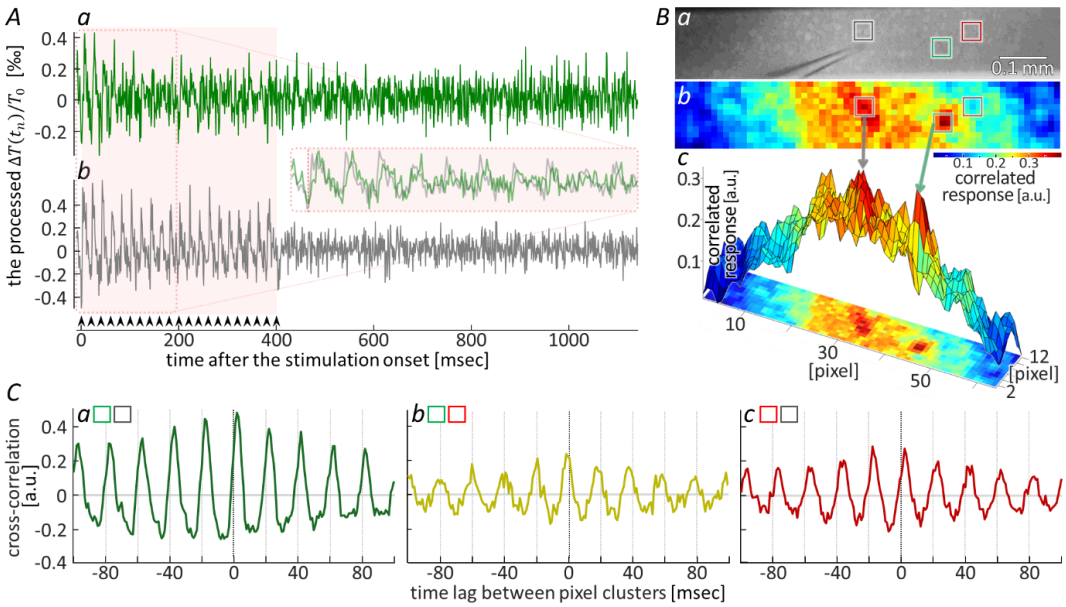


Figure 3. Deconvolved activities of neuronal elements. *A*) Local response time courses for the pixel clusters indicated by the *green* and *black* squares in *B-ab*. Inset: Superimposition of time-course segments encircled by the *dotted* rectangle. *B*) Spatial correlation map for the particular pixel cluster indicated by the *green* square in *B-ab*. *C*) Temporal cross-correlation functions for three different pairs of 3×3-pixel areas: pair of *green* and *grey* squares in *B-ab* (*a*), pair of *green* and *red* squares (*b*), and pair of *green* and *grey* squares (*c*).

arrowheads in panel *A*), and the subsequent analyses were conducted over this time period.

Figure 3*C-a* shows the temporal cross-correlation function between the two response time courses, demonstrating temporally correlated 50-Hz activity with a 2-msec time lag between the responses. For comparison, a temporal cross-correlation function was also calculated between the selected pixel cluster (*green* square in panel *B-ab*) and a nearby pixel region (*red* square in panel *B-ab*) that showed relatively low correlation with the selected cluster, despite its spatial proximity (Figure 3*C-b*). A cross-correlation function was calculated between this example pixel region and the pixel cluster near the stimulating electrode tip (*black* square in panel *B-ab*). In both cases, the cross-correlation amplitude was significantly lower than that observed for the pair of pixel clusters exhibiting prominent peaks on the spatial correlation map (i.e., the clusters indicated by *green* and *black* squares). This result supports the interpretation that the specific pattern observed in the spatial correlation map reflects the functional coupling of neuronal elements associated with the selected pixel cluster.

In the results discussed above, a specific pixel cluster was manually selected to ensure, through visual inspection, the presence of distinct VSD signals clearly contrasted with the surrounding areas (e.g., *white* squares in Figure 2). This step may be required in certain situations, such as when the signal-to-noise ratio is insufficient and/or spatially inhomogeneous due to uneven staining of the tissue with the dye. However, such manual selection could introduce subjective bias into the subsequent analyses. Therefore, we additionally explored an alternative image processing workflow, as illustrated in Figure 1. In this workflow, spatial cross-correlation maps were computed for every pixel in the image frame, excluding those located along the image boundaries, resulting in a total of 620 maps (corresponding to 10 × 62 pixels). Among these maps, specific patterns of correspondence were observed across multiple maps generated from different reference pixels.

Figure 4 depicts two representative examples of such spatial cross-correlation maps, with the reference pixels indicated by *white* asterisks. Both maps display patchy clusters of pixels exhibiting relatively high correlation values, including areas surrounding the reference pixel. Although the majority of these clusters are located near the stimulation site in each map, one cluster appears at a distance from the reference pixel, indicated by an arrow. Notably, the position of this distant cluster relative to the reference pixel in one map corresponds to the position of the reference pixel relative to the distant cluster in the other map. Such a correspondence across different maps may reflect shared or overlapping circuit dynamics between spatially separated regions.

4. Discussion

Following the proposed method (Figure 1), local neuronal activities evoked by the stimulus, previously obscured by the global neural response, were visually highlighted in the time-series images (Figure 2). This enabled the extraction of both spatial correlation maps and temporal cross-correlation functions from selected pixel regions (Figure 3). Additionally, an alternative

DOI: https://doi.org/10.22452/mjs.vol45sp2.4
Malaysian Journal of Science 45 (Special Issue 2): 37-42 (November 2026)

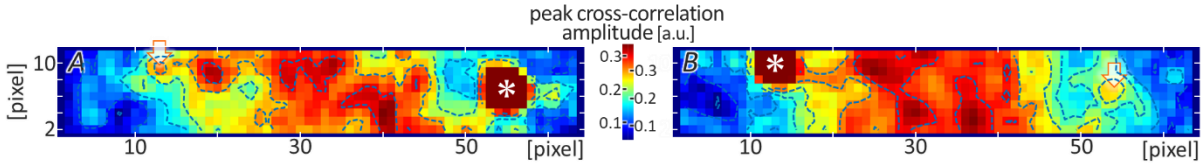


Figure 4. Spatial cross-correlation maps computed using different reference pixels. Each *white* asterisk in panels *A* and *B* indicates the reference pixel used to compute the corresponding map. Contour lines are overlaid on the color maps to highlight spatial patterns. Color bars indicate the peak amplitude of the temporal cross-correlation. Both the horizontal and vertical axes represent pixel indices.

image processing workflow was introduced to generate spatial cross-correlation maps, using any pixel in the imaging field as a reference (Figure 4). In each map, spatially discernible patchy structures, each less than 100 micrometers in diameter, were displayed.

We focused exclusively on image frames that captured neural activity during pulse-train stimulation. Baseline and post-stimulus activities, as well as responses to other types of stimulation, were not examined. Consequently, the present approach does not account for intrinsic functional coupling across different neural conditions. Moreover, the current method depends on manual comparisons of the generated spatial correlation maps (Figure 4). Therefore, further development is necessary to establish an efficient strategy for grouping similar correlation maps, such as through statistical segmentation or other suitable techniques, and for subsequently performing automatic deconvolution of neuronal components.

The validation of the proposed method is primarily qualitative. Incorporating comparisons with ground-truth neuronal recordings would increase the credibility of our approach. However, since VSD imaging captures voltage changes across all cytoplasmic membranes within the three-dimensional volume of the imaging field, obtaining direct neuronal recordings would require the placement of electrodes throughout the entire field of view, which is not practically feasible. Recent studies have introduced deconvolution methods for VSD imaging data (e.g., Benisty et al., 2022). However, these approaches have mainly focused on extracting action potentials from individual neurons rather than on revealing functional connectivity among neuronal elements. Furthermore, some of these methods assume that individual somata are already visible in the imaging data (e.g., Xie et al., 2021), which restricts their applicability to our experimental conditions. An alternative approach that may be feasible in our case is the use of confocal imaging with Ca^{2+}-sensitive dyes (cf. Tanaka et al., 2019), which can provide three-dimensional localization of neuronal somata. Further investigation is justified in this direction.

5. Conclusion

To the best of our knowledge, this study is the first to attempt the deconvolution of functional connectivity between neuronal ensembles responding to microstimulation, based on macroscopic VSD imaging data, through spatio-temporal cross-correlation analyses. The present findings suggest the feasibility of the proposed method as a tool for dissecting cortical network dynamics in response to microstimulation and, ultimately, for optimizing stimulation protocols for visual prostheses.

6. Acknowledgements

This research was supported in part by Grant-in-Aid for Scientific Research from MEXT, Japan (22K12781, 25K15892 to Y.H.), and JST SPRING, Japan (JPMJSP2137 to Mie Univ./S.F.).

7. References

Benisty H., Song A., Mishne G., Charles A. S. (2022) Review of data processing of functional optical microscopy for neuroscience, *Neuro-photonics*, 9 (4): 041402 (32 pp.).

Chen X., Wang F., Fernández E., Roelfsema P. R. (2020) Shape perception via a high-channel-count neuroprosthesis in monkey visual cortex, *Science* 370 (6521): 1191-1196.

Fehérvári T. D., Okazaki Y., Sawai H., Yagi T. (2015) In vivo voltage-sensitive dye study of lateral spreading of cortical activity in mouse primary visual cortex induced by a current impulse, *PLoS One* 10 (7): e0133853 (24 pp.).

Fernández E., Alfaro A., Soto-Sánchez C., Gonzalez-Lopez P., Lozano A. M., Peña S., Grima M.D., Rodil A., Gómez B., Chen X., Roelfsema P. R., Rolston J. D., Davis T. S., Normann R. A. (2021) Visual percepts evoked with an intracortical 96-channel microelec-trode array inserted in human occipital cortex, *J. Clin. Invest.* 131 (23): e151331 (15 pp.).

Fukuda S., Nomoto T., Yoshida K., Hayashida Y., Yagi T. (2021) Accumulation of non-synaptic and synaptic excitations induced by microstimulation pulses in the mouse visual cortex layer II/III, *2021 43rd Ann. Int'l Conf. I.E.E.E. Med. Biol. Soc.*: 5152.

Fukuda S., Yoshida K., Nomoto T., Yagi T., Hayashida Y. (2022) Use-dependent inactivation of the mouse visual cortex in response to microstimulation train, *2022 E-Health Bioeng. Conf.*: 1-4.

Hayashida Y., Takeuchi K., Ishikawa N., Okazaki Y., Fehérvári T. D., Tanaka H., Yagi T. (2014) Voltage-sensitive dye imaging of the visual cortices responding to electrical pulses at different intervals in mice in vivo, 2014 36th *Ann. Int'l Conf. I.E.E.E. Med. Biol. Soc.*: 402-405.

DOI: https://doi.org/10.22452/mjs.vol45sp2.4
Malaysian Journal of Science 45 (Special Issue 2): 37-42 (November 2026)

Hayashida Y., Kameda S., Umehira Y., Ishikawa S., Yagi T. (2022) Multichannel stimulation module as a tool for animal studies on cortical neural pros-theses, *Front. Med. Technol.* 4: 927851 (21 pp.).

Miyamoto S., Suematsu N., Umehira Y., Hayashida Y., Yagi T. (2017) Age-related changes in the spatiotemporal responses to electrical stimulation in the visual cortex of rats with progressive vision loss, *Sci. Rep.* 7(1): 14165 (13 pp.).

Nomoto T., Tanaka Y., Hayashida Y., Yagi T. (2017) Imaging of population spikes induced by repetitive stimulus pulses in mouse cerebral slices in vitro, *2017 39th Ann. Int'l Conf. I.E.E.E. Med. Biol. Soc.*: 1109.

Schmidt E. M., Bak M. J., F T Hambrecht, C V Kufta, D K O'Rourke, P Vallabhanath (1996) Feasibility of a visual prosthesis for the blind based on intracortical microstimulation of the visual cortex, *Brain* 119 (2): 507-522.

Tanaka Y., Nomoto T., Shiki T., Sakata Y., Shimada Y., Hayashida Y., Yagi T. (2019) Focal activation of neuronal circuits induced by microstimulation in the visual cortex, *J. Neural Eng.* 16 (3): 036007 (17 pp.).

Xie M. E., Adam Y., Fan L. Z., Böhm U. L., Kinsella I., Zhou D., Rozsa M., Singh A., Svoboda K., Paninski L., Cohen A. E. (2021) High-fidelity estimates of spikes and subthreshold waveforms from 1-photon voltage imaging in vivo, *Cell Reports* 35(1): 108954 (15 pp.).

DOI: https://doi.org/10.22452/mjs.vol45sp2.4
Malaysian Journal of Science 45 (Special Issue 2): 37-42 (November 2026)